AIP | Applied Physics Letters

Hybrid whispering gallery mode/plasmonic chain ring resonators for biosensing

Ehsan Arbabi, Seyedeh Mahsa Kamali, Stephen Arnold, and Lynford L. Goddard

Citation: Applied Physics Letters **105**, 231107 (2014); doi: 10.1063/1.4903876
View online: http://dx.doi.org/10.1063/1.4903876
View Table of Contents: http://scitation.aip.org/content/aip/journal/apl/105/23?ver=pdfcov
Published by the AIP Publishing

Hybrid whispering gallery mode/plasmonic chain ring resonators for biosensing

Ehsan Arbabi,[1] Seyedeh Mahsa Kamali,[1] Stephen Arnold,[2] and Lynford L. Goddard[1,a)]
[1]*Micro and Nanotechnology Laboratory, Department of Electrical and Computer Engineering, University of Illinois at Urbana-Champaign, Urbana, Illinois 61801, USA*
[2]*MicroParticle PhotoPhysics Lab, NYU Polytechnic School of Engineering, Brooklyn, New York 11201, USA*

(Received 14 October 2014; accepted 28 November 2014; published online 9 December 2014)

We analyze the physics of hybrid whispering gallery mode resonators formed by arranging a periodic array of epitopes (i.e., gold nano-shells covering silica nano-spheres) around the equator of a silica microsphere. When the epitopes are located at the antinodes of the field of the whispering gallery mode, we find that the field localization properties near the epitopes change drastically as the radius of the epitopes is varied due to the existence of distinct coupling regions of the hybrid resonator. We investigated the application of such resonators for biosensing by calculating the resonance wavelength shift caused by a binding event of a single Thyroglobulin cancer marker protein to the surface of an epitope in the chain. © *2014 AIP Publishing LLC*.
[http://dx.doi.org/10.1063/1.4903876]

Applications of whispering gallery mode (WGM)[1,2] and nano-plasmonic resonators[3] as high sensitivity label free biosensors are well known. A more recent structure that combines the benefits of the two is the hybrid WGM-plasmonic resonator or WGM-h.[4,5] Utilizing both the high quality factors of WGM microcavities and the large field enhancements of local surface plasmon (LSP) resonators, these structures have enabled unprecedented sensitivities. A major drawback of this structure is the long time intervals between bio-agent adsorptions, as well as the waiting time for the first detection. This is mostly due to the small adsorption area with high field enhancement available on the LSP resonator. Forming a periodic chain of similar plasmonic resonators around the equator of a WGM resonator can effectively scale up the adsorption surface area and reduce the detection time intervals.[6]

One possible arrangement consists of a WGM microcavity with two LSP resonators per each period of the WGM mode of interest. This structure has been previously studied using a perturbation method,[6] where it was shown that the degeneracy between the two counter-propagating WGM modes is lifted and two standing waves are formed. For one of these standing waves, the electric field amplitude is maximum at the epitopes, while for the other one, it is close to zero around them (Fig. 1). We call these the antinode mode and the node mode, respectively. We focus on analyzing the behavior of the antinode mode since it is more important for biosensing applications due to the large field enhancement near the epitopes. This intense electric field results in a considerable resonance shift after a binding event and thereby improves sensitivity. We also study the WGM-h structure with fewer epitopes around the equator. For instance, we can have only one epitope per two periods of the WGM field.

The TE_r (transverse electric with respect to r) antinode mode of the WGM-h structure can be efficiently simulated using periodic boundary conditions in the azimuthal direction, i.e., the perfect electric conductor (PEC) and perfect magnetic conductor (PMC) boundaries shown in Fig. 2. The simulation domain can be reduced further by using the symmetry with respect to the equatorial plane, i.e., we use a PEC boundary on this plane and then only simulate the region above the plane. These symmetries considerably reduce the memory and time required to execute the simulations and make an otherwise impossible task feasible on a personal workstation. In addition, since the WGM modes of interest are confined close to the equatorial line of the microsphere, we can limit the simulation domain to a few micrometers near the equatorial line. Using this set of simplifications, the TE_r antinode mode of the WGM-h can be efficiently found.

Here, we consider a 32 μm radius silica microsphere suspended in water as the WGM resonator and epitopes consisting of gold nano-shells covering silica nano-spheres as the LSP resonators, similar to a previous study.[5] The described WGM microcavity operates near 778.5 nm with an azimuthal mode number of M = 364 (for the lowest order WGM mode). We will denote the radius of the silica nano-spheres (which is equal to the inner radius of gold nano-shells) by r_1 and the outer radius of the epitopes by r_2, with $t = r_2 - r_1$ denoting the thickness of the shells. In this letter, we will set $t = 10$ nm for simplicity. For a structure with two epitopes

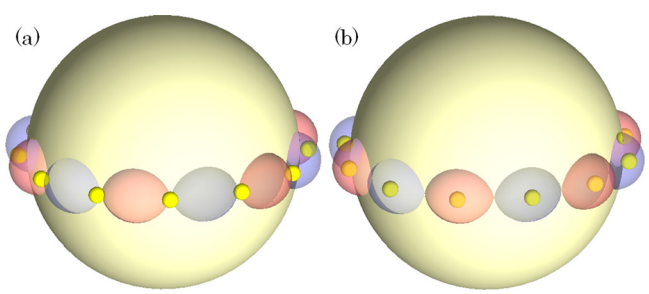

FIG. 1. (a) Node and (b) antinode modes showing the electric field profile relative to the plasmonic resonator locations.

a)Author to whom correspondence should be addressed. Electronic mail: lgoddard@illinois.edu

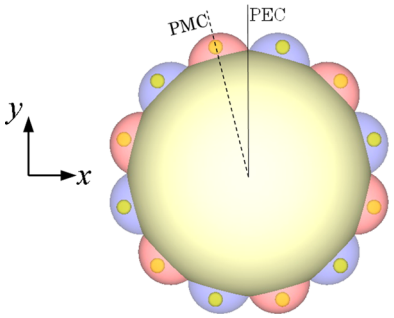

FIG. 2. Top view showing the PEC (solid line) and PMC (dashed line) boundaries for simulation.

per period of the WGM mode, there are a total of N = 728 epitopes around the equator.

The electric field distribution and polarization on a log scale at an antinode azimuthal plane for $r_1 = 30\,\text{nm}$ are shown in Fig. 3. The resonance wavelength of this WGM-h is $\lambda_h = 779.36\,\text{nm}$. This is higher than that of a bare WGM microcavity ($\lambda_{bare} = 778.5\,\text{nm}$) and shows that these epitopes have a positive effective polarizability. The quality factor of the WGM-h is $Q_h = 4900$, whereas the bare microcavity has $Q_{bare} = 2.4 \times 10^6$. Using the reactive sensing formula,[7] we can calculate the change in the resonance wavelength that results from a single bio-agent binding to one of the epitopes of the WGM-h

$$\frac{\delta\lambda_h}{\lambda_h} = -\frac{\delta\omega_h}{\omega_h} = \frac{\int \delta\left(n^2(\boldsymbol{r})\right) E(\boldsymbol{r}) \cdot E_0^*(\boldsymbol{r}) dV}{2\int n^2(\boldsymbol{r}) |E_0(\boldsymbol{r})|^2 dV}, \qquad (1)$$

where λ_h and ω_h are the initial resonance wavelength and angular frequency of the WGM-h before binding, $\delta\lambda_h$ and $\delta\omega_h$ are the changes in these parameters due to a binding, $n^2(\boldsymbol{r})$ is the relative permittivity, $\delta(n^2(\boldsymbol{r}))$ is its change due to binding, and $\boldsymbol{E}_0(\boldsymbol{r})$ and $\boldsymbol{E}(\boldsymbol{r})$ are the electric fields of the WGM-h before and after binding, respectively. The integrand in the numerator is non-zero only in the volume of the binding agent. To estimate the resonance shifts, we model the Thyroglobulin (Tg) cancer marker protein as an oblate spheroid of axes 11 nm and 5.5 nm with a refractive index of ~1.5.[5] We assume that the Tg protein is attached to the upper pole of the plasmonic epitope, where the maximum field enhancement occurs in the TE_r mode. In this case, a resonance shift of $\delta\lambda_h = 0.9\text{fm}$ is calculated. This is a significant enhancement compared to a bare silica microsphere, which has a theoretical shift of $\delta\lambda_{bare} \sim 0.06\text{fm}$.[5,7] As can be seen in Fig. 3(a), the electric field distribution is very close to that of a bare microsphere, and it is only slightly perturbed by the presence of the epitopes.

For a larger epitope with $r_1 = 50\,\text{nm}$, the electric field intensity is plotted in Fig. 3(b). We see a negative effective polarizability since $\lambda_h = 777.79\,\text{nm}$. The quality factor is $Q_h = 3680$. A shift of $\delta\lambda_h = 0.2\text{fm}$ is calculated for a single Tg protein binding. The field is very close to that of a bare WGM microsphere in this case as well, and only a perturbation with a negative polarizability is added.

Although the epitopes can be treated as a perturbation for these sets of sizes, this is not the case for some other sizes. For instance, if $r_1 = 40\,\text{nm}$, two different modes with different properties are found instead of one. The electric field intensity distributions are plotted in Fig. 3(c) for the two modes that arise. We will call the mode that is plotted in Fig. 3(c-i) and has a longer $\lambda_h = 787.19\,\text{nm}$, the symmetric mode, and the other one with $\lambda_h = 776.45\,\text{nm}$ shown in Fig. 3(c-ii), the anti-symmetric mode. As can be seen in the plots, a higher field enhancement around the epitope is achieved for the symmetric mode where $\delta\lambda_h = 16.7\text{fm}$ is calculated for a Tg binding. However, the quality factor drops very significantly, to $Q_h = 90$, because the electric field is highly localized around the lossy plasmonic epitopes. For the anti-symmetric mode, the resonance shift was only $\delta\lambda_h = 1.44\text{fm}$, but the quality factor only dropped to $Q_h = 1180$.

For these dimensions, we see that changes resulting from the presence of the epitopes are considerable and the epitopes cannot be treated merely as a perturbation. A strong coupling is observed between the WGM microsphere and the chain of epitopes. The appearance of two modes implies that there must have been two separate resonant modes initially that became coupled to each other. While the fundamental TE_r mode of the WGM resonator is one of the initial modes, the other one is that of the *plasmonic chain ring resonator (PCRR)*. In general, a chain of periodically coupled resonators can form a wave-guiding structure with different Bloch modes.[8] It has been previously observed that a periodic linear arrangement of plasmonic nano-resonators can form a waveguide with long range interparticle coupling[9] resulting in certain modes and wavenumbers.[9,10] Therefore, we can expect that an optical resonator is formed, when such a chain is bent to construct a PCRR.[11] To confirm that the coupling

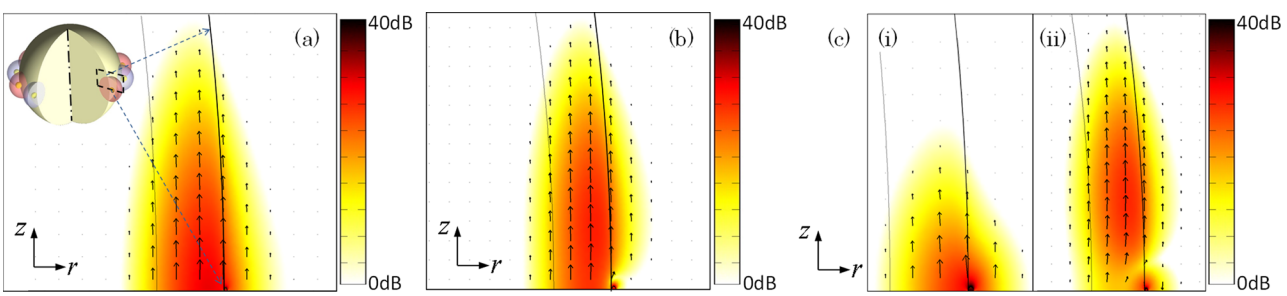

FIG. 3. Electric field distribution at the cross section of the microsphere close to an epitope for $t = 10\,\text{nm}$ and (a) $r_1 = 30\,\text{nm}$, (b) $r_1 = 50\,\text{nm}$, and (c) $r_1 = 40\,\text{nm}$, which has two modes: (i) symmetric and (ii) anti-symmetric. The thick solid curved line in each figure shows the surface of the silica microsphere. The thinner curved line to the left of the thick line (i.e., inside the microsphere) only serves to define various mesh sizes.

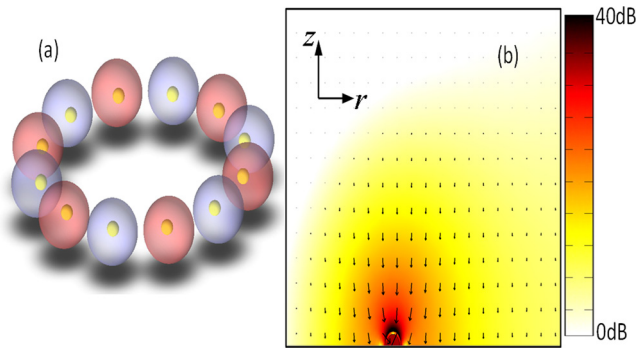

FIG. 4. (a) Schematic of the PCRR and standing wave field distribution and (b) electric field distribution around an epitope in the PCRR.

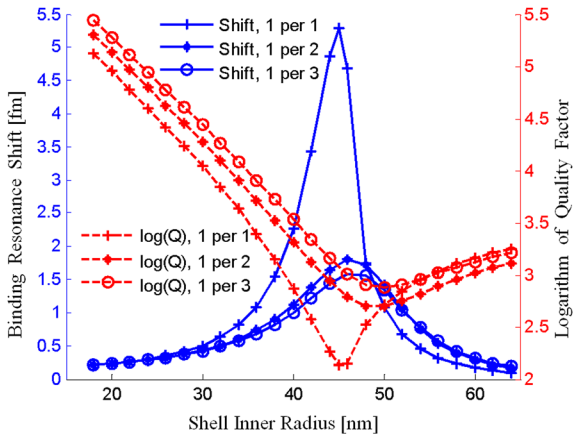

FIG. 6. Resonance wavelength shifts, $\delta\lambda_h$, due to a single Tg binding event (left axis) and quality factors on a logarithmic scale, $\log_{10}(Q_h)$ and (right axis) for WGM-h resonators with one epitope per 1, 2, and 3 periods of the WGM field.

of the WGM and the PCRR is responsible for generating the symmetric and anti-symmetric modes, we analyzed rings formed solely with epitopes for different radii. For $r_1 = 40\,\text{nm}$ and $t = 10\,\text{nm}$, the electric field distribution of the PCRR mode with a wavenumber of 364 (the one that couples to the desired WGM mode effectively) is plotted in Fig. 4.

We calculated the resonance wavelengths, the shifts due to a single binding event, and the quality factors for the symmetric and anti-symmetric modes of the WGM-h resonator for a range of r_1 values while keeping t constant at 10 nm. The results can be seen in Fig. 5. For small epitopes, i.e., for $r_1 < 36\,\text{nm}$, the resonance wavelength of the symmetric mode is very close to that of the bare WGM microcavity, and the field distribution of the two modes are also very similar. However, for $r_1 > 42\,\text{nm}$, it is the anti-symmetric mode that has a resonance wavelength close to that of the bare WGM microcavity, and although the fields seem different, the anti-symmetric mode can still be viewed as the WGM mode perturbed by a chain of epitopes with negative polarizability. We are in a weak coupling regime when $r_1 < 36\,\text{nm}$ or $r_1 > 42\,\text{nm}$, whereas in the region in between, the coupling is strong and the WGM-h modes become significantly different than both the WGM mode and the PCRR standalone mode.

There is one apparent inconsistency with this simple analysis. Although the field profile of the symmetric mode for $r_1 > 42\,\text{nm}$ becomes similar to that of the standalone PCRR mode, their resonance wavelengths do not agree, not even asymptotically. The reason can be traced back to the presence of the large silica microsphere that considerably alters the effective index of the surrounding environment. That is, the resonance wavelength of a PCRR *perturbed* by the presence of a large silica microsphere is different than that of a PCRR without the microsphere. It is this perturbed resonance wavelength that must asymptotically behave like that of the symmetric mode of the hybrid resonator. We have plotted an estimation of the resonance wavelength of the PCRR with this correction in Fig. 5(a).

Based on these observations, we have established three different regimes for the hybrid WGM-PCRR: a symmetric weak coupling regime, an anti-symmetric weak coupling regime, and a strong coupling regime with both modes. The binding resonance shifts of the WGM-h in each regime are shown in Fig. 5(b). Figure 5(c) shows the corresponding quality factors. The greatest shifts occur for the symmetric mode in the strong coupling regime; however, this is also exactly where the resonator has a very low quality factor.

Some other cases of interest arise when there are fewer plasmonic epitopes in the chain, e.g., one epitope per 1, 2, or 3 periods of the WGM field or even just a solitary epitope. We expect the behavior of the WGM-h hybrid resonator to be fundamentally different in these cases than in the two epitopes per period case because the spacing between adjacent epitopes is too large to form a PCRR that is resonant near the operating wavelength. Thus, symmetric and anti-symmetric modes will not form in the WGM-h.

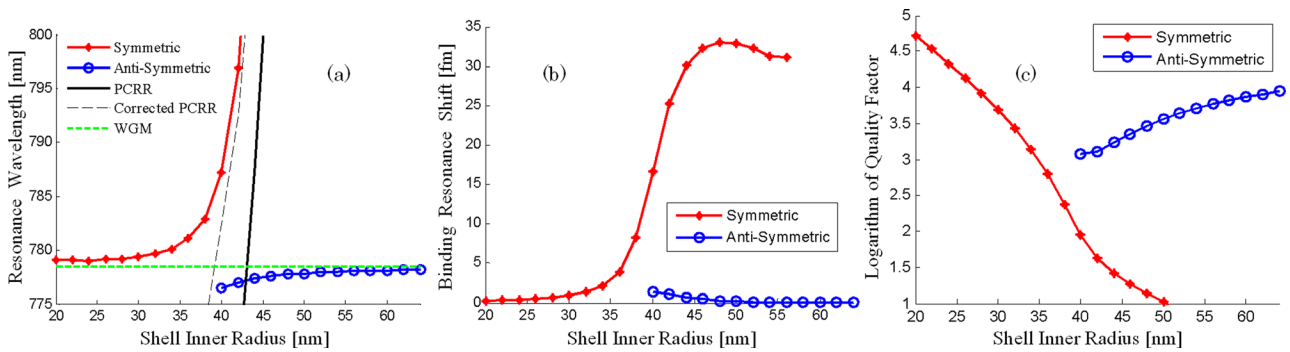

FIG. 5. (a) Resonance wavelengths, λ_h, of the symmetric mode, anti-symmetric mode, PCRR, and WGM. The corrected PCRR curve estimates λ_h for a PCRR perturbed by a silica microsphere. (b) Resonance wavelength shifts, $\delta\lambda_h$, due to a single Tg protein binding for the symmetric and the anti-symmetric modes. (c) Corresponding quality factors on a logarithmic scale, i.e., $\log_{10}(Q_h)$.

The binding resonance shifts and the quality factors for three repetition rates are shown in Fig. 6. For very small ($r_1 < 32$ nm) or very large ($r_1 > 52$ nm) epitopes, the resonance shift curves are very close; the quality factor curves are offset by a nearly constant amount because the total number of lossy epitopes increases with the repetition rate. However, the differences are quite significant when the radius is close to where the maximum shift and lowest quality factor occurs. This is to be expected since this is where the most efficient coupling between the WGM microsphere and the epitopes occurs. Hence, a binding event on a single epitope has a collective effect on the entire epitope chain and simulation accuracy will be sacrificed if the epitopes are treated as isolated perturbations. For most epitope dimensions and repetition rates, however, the curves are very close because the epitopes are only weakly coupled and thus they behave like isolated perturbations. This implies that in the case of only one epitope attached to the WGM microsphere, the shift due to a binding event will be comparable to Fig. 6 results for the one epitope per 3 period cases, but the quality factor for the solitary epitope case will be orders of magnitude larger. These are two important conclusions of the analysis presented in this letter because the WGM-h simulation with a single epitope is computationally intractable since periodic boundary conditions cannot be used.

When designing a WGM-h sensor for detecting a single binding event of a small volume bio-agent, such as Tg, three key parameters to consider are: the binding shift, quality factor, and detection interval, in addition to the measuring instrument's capabilities. Figures 5(b), 5(c), and 6 can be used to select a suitable sensor design that balances these tradeoffs. For fixed epitope dimensions, the single epitope WGM-h has a high quality factor but a long detection interval since there is only one binding site, while the periodic array of weakly coupled epitopes has a lower quality factor, a comparable binding shift, but a detection interval scaled down by the number of epitopes. In short, the quality factor can be sacrificed for an improved detection interval by increasing the repetition rate. The WGM-h with two epitopes per period of the WGM mode has the lowest quality factor but the shortest detection interval and largest binding shift of structures studied here. The quality factor can be increased by selecting small or large epitope dimensions ($r_1 < 36$ nm or $r_1 > 42$ nm) in exchange for a smaller binding shift. Thus, the WGM-h with two epitopes per period can be a potential candidate to solve the problem of long detection intervals, while balancing the tradeoff of having a large wavelength shift from binding and having a narrow resonance.

Various imperfections may occur when fabricating the WGM-h resonator. A WGM microcavity fabricated with a different radius or refractive index will have a different resonance wavelength for its M = 364 mode. Since the characteristics of the plasmonic epitopes also vary with their size, we can expect a WGM-h resonator with small fabrication errors to behave as before, but with the shell inner radius axis shifted in each figure. Another issue might arise because of variations in the sizes of the epitopes or errors in their placements. We can expect that small deviations can be modeled using a perturbational approach. These imperfections will modify the resonance wavelength and quality factor of the hybrid resonator because of added scattering. In addition, the magnitude of the binding wavelength shift may depend on the size of the epitope to which the protein binds.

In conclusion, we studied the behavior of hybrid resonators formed by arranging a periodic array of plasmonic epitopes around a WGM micro-resonator. In structures with two epitopes per period of the WGM mode, we observed three different coupling regimes: weak symmetric coupling (in phase), weak anti-symmetric coupling (where WGM and PCRR modes are 180° out of phase), and strong coupling (with both the symmetric and anti-symmetric modes). In cases with fewer epitopes, such as one epitope per 1, 2, or 3 periods, the spacing between the epitopes is too large to form a PCRR that is resonant near the operating wavelength and so we only observe one mode, namely, the TE_r mode of the WGM resonator perturbed by the epitope chain. For most dimensions and repetition rates, the epitopes are weakly coupled. Thus, a binding event does not produce a collective effect in the chain, and consequently, the shift is comparable to that from a WGM-h resonator with a single epitope.

This work was supported in part by the National Science Foundation CAREER Award ECCS-1055941 with matching funds from the University of Illinois. S.A. was supported by NSF Award ECCS-1303499.

[1]F. Vollmer and S. Arnold, Nat. Methods **5**, 591 (2008).
[2]M. S. Luchansky and R. C. Bailey, Anal. Chem. **84**, 793 (2012).
[3]I. Ament, J. Prasad, A. Henkel, S. Schmachtel, and C. Sönnichsen, Nano Lett. **12**, 1092 (2012).
[4]S. I. Shopova, R. Rajmangal, S. Holler, and S. Arnold, Appl. Phys. Lett. **98**, 243104 (2011).
[5]V. R. Dantham, S. Holler, C. Barbre, D. Keng, V. Kolchenko, and S. Arnold, Nano Lett. **13**, 3347 (2013).
[6]S. Arnold, V. R. Dantham, C. Barbre, B. A. Garetz, and X. Fan, Opt. Express **20**, 26147 (2012).
[7]S. Arnold, M. Khoshsima, I. Teraoka, S. Holler, and F. Vollmer, Opt. Lett. **28**, 272 (2003).
[8]A. Yariv, Y. Xu, R. K. Lee, and A. Scherer, Opt. Lett. **24**, 711 (1999).
[9]D. S. Citrin, Nano Lett. **5**, 985 (2005).
[10]S. Raeis Zadeh Bajestani, M. Shahabadi, and N. Talebi, J. Opt. Soc. Am. B **28**, 937 (2011).
[11]D. S. Citrin, J. Opt. Soc. Am. B **22**, 1763 (2005).